SUPPLEMENTARY MATERIALS

TABLE OF CONTENTS

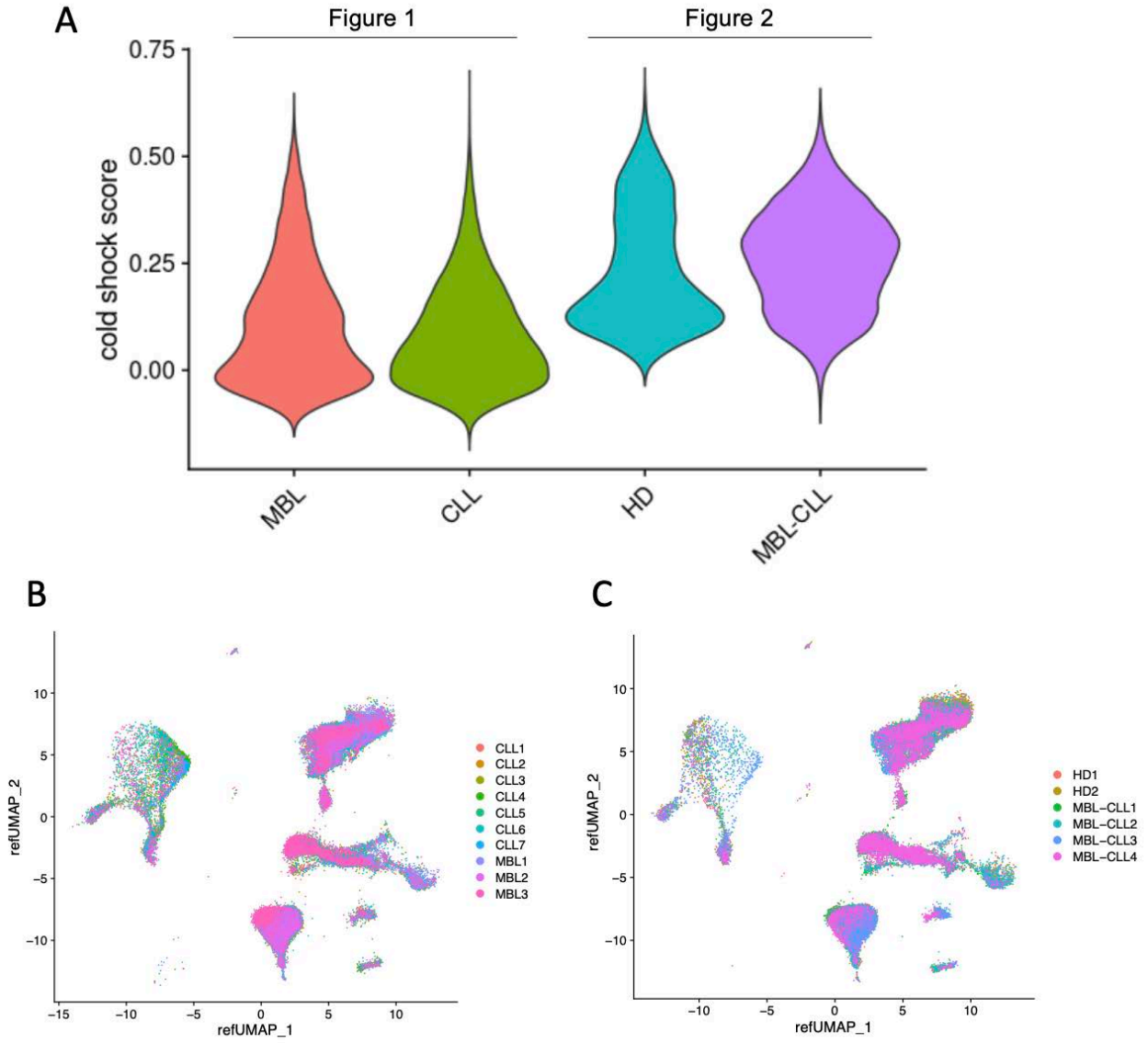

Supplementary Figure 1: Patient cohort selection and integration. (**A**) Cold-shock signatures for each patient cohort. We analyzed 3 non-progressive MBL patients and 7 CLL patients together in Figure 1 due to their similar cold-shock signature scores. Similarly, for Figure 2, our comparisons consisted of 4 paired MBL-CLL patients with 2 healthy donors given their equivalent cold-shock signature scores. (**B**) UMAP visualization by patient ID for samples analyzed in Figure 1. (**C**) UMAP visualization by patient ID for samples analyzed in Figure 2. The high degree of integration of patients in each cluster indicates the lack of batch effect.

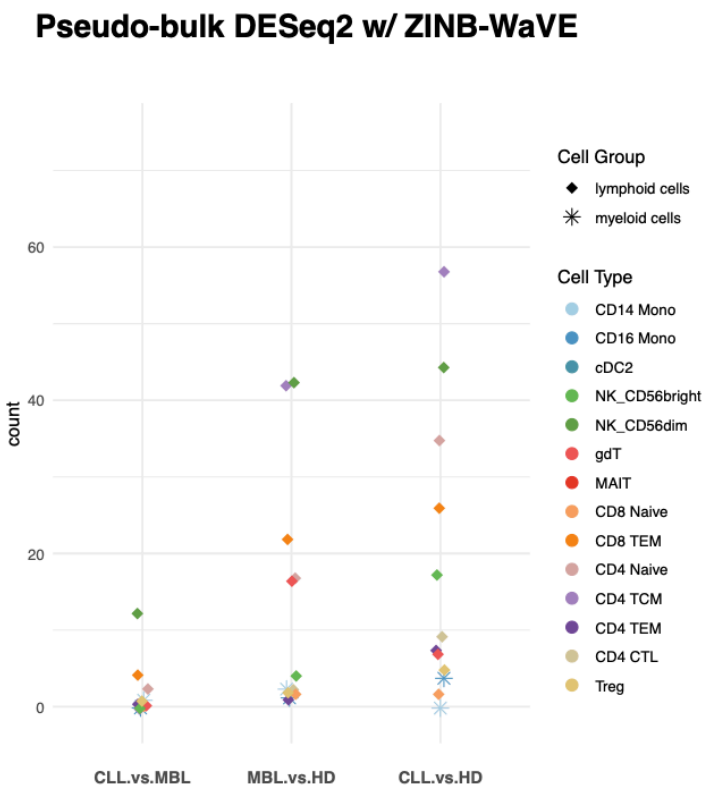

Supplementary Figure 2. Number of significant expressed genes with pseudo-bulk analysis. Zero-inflated negative binomial-based wanted variation extraction method (ZINB-WaVE) was applied to the pseudo-bulk raw count before applying the DESeq2 tool for differential gene analysis. Cells were categorized based on lymphoid and myeloid cells.

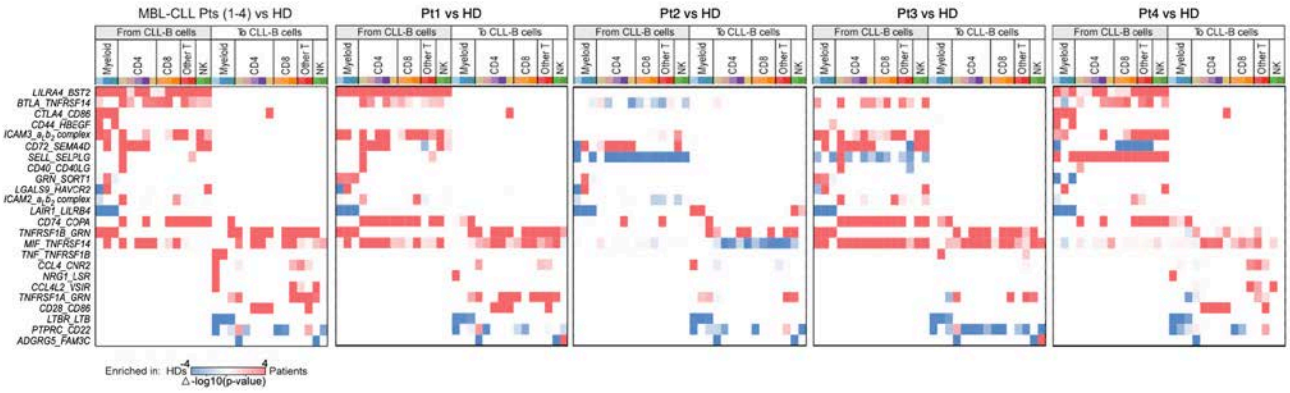

Supplementary Figure 3. Receptor and ligand expression showing enrichment of interactions on a per-individual patient basis. Heatmaps representing the difference of p-values for each ligand-receptor pair for specific cell types. From left to right: All patients and individual patients 1-4 compared to healthy donors. Abbreviations: Pt: Patient; HD: Healthy donor.

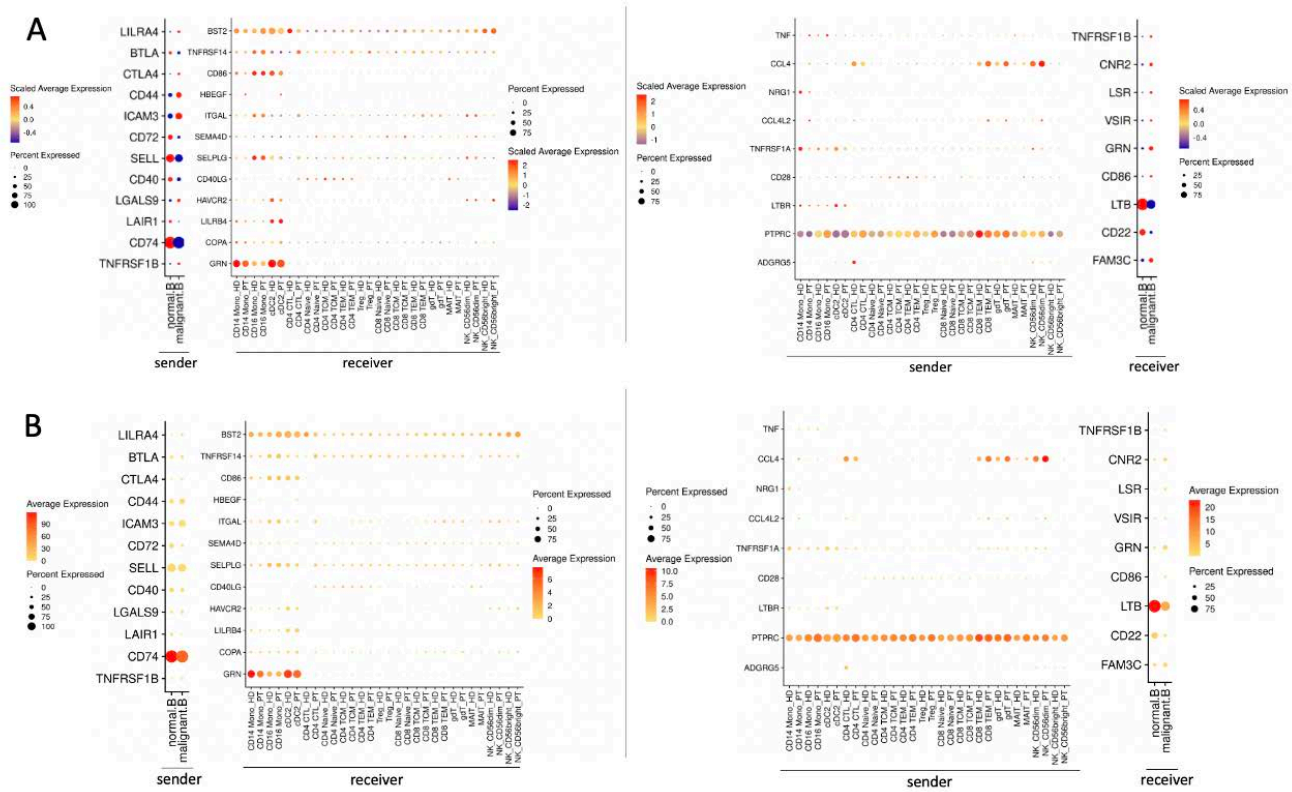

Supplementary Figure 4. Receptor and ligand expression levels and percentages of expressing cells. Receptor and ligand expression based on scaled (z-score) expression levels (**A**) or unscaled expression levels (**B**) in receiver and sender cells. Dot size represents the percentage of cells expressing that gene. Expression from healthy donors and from patients are placed next to each other for comparison. Abbreviations: PT: Patient; HD: Healthy donor.

METHODS

Human CLL and MBL samples

Serial samples from MBL patients that progressed to CLL, non-progressive MBL, and CLL patients along with PBMCs from healthy individuals were collected in accordance with the Declaration of Helsinki and written informed consent was obtained from all participants.

Heparinized blood was collected, and PBMCs were isolated by Ficoll/Hypaque density gradient centrifugation and cryopreserved with FBS and 10% DMSO and stored in vapor-phase liquid nitrogen until the time of analysis.

Sample processing for single cell analysis

Cells were thawed in Roswell Park Memorial Institute (RPMI) 1640 medium supplemented with 10% fetal bovine serum (FBS) and centrifuge at 1,500rpm for 5 minutes. Each sample was filtered through a 70μm filter. Cells were re-suspended in PBS-0.04% bovine serum albumin (BSA) and stained with anti-human CD5 (fluorescein isothiocyanate [FITC]), CD19 (Phycoerythrin-cyanine-7 [PE-Cy7]) and 7-aminoactinomycin D (7-AAD) for 15 minutes on ice (Biolegend). The samples were washed and re-suspended in PBS-0.04% BSA at a concentration of $10x10^6$ cells/mL. Samples from the same patient were processed and sorted in parallel on the same day using two FacsAria II cytometers (Becton Dickinson [BD]). Cells were sorted through a 70μm nozzle into 1.5mL Eppendorf tubes with 10μL PBS-0.04% BSA and immediately stored on ice. Cellular suspensions were loaded on a GemCode Single-Cell Instrument (10x Genomics, Pleasanton, CA, USA) to generate single-cell Gel bead in Emulsion (GEM). Single-cell RNA-seq libraries were prepared as previously described[1].

Alignment, barcode assignment and UMI counting

scRNA-seq reads from each sample were processed, aligned to the Hg19 reference genome and filtered using the CellRanger pipeline (v. 3.1.0). Raw feature-barcode matrices were used for further analysis for each sample.

Single-cell Data Quality Control and Cell Clustering

Initial quality control was conducted using Seurat V4.0.0 with following criteria: cells with 500<genes<3000 were retained and any with >10% mitochondrial reads were excluded. Genes were filtered by retaining the ones with expression at least in 5 cells. We assessed the 'cold-shock signature'[2] for each sample to assess potential processing and batch artefacts between samples and cohorts due to cryopreservation. We selected cohorts with similar cold-shock signature for comparison (**Supplementary Figure 1A**). As a result, 3 non-progressive MBL samples and 7 CLL patients were selected to be analyzed together (**Figure 1**) and the 4 paired-sample MBL-CLL patients were analyzed with HDs (**Figure 2**).

With each analysis cohort after quality control, we isolated non-tumor population after performing standard Seurat clustering with first 30 principal components. We assigned non-tumor cell types by performing multimodal reference mapping with CITE-seq reference of 162,000 PBMC measured with 228 antibodies[3]. The immune cell type composition was calculated based on the weighted average number of each immune cell type from all patients in each condition. Same quality control and analysis pipelines were used for the 2 samples with Ibrutinib treatment. For the CLL6 sample[4], the post-treatment sample includes cells from day 30, 120, and 280 after treatment. These cells were combined in order to obtain a sufficient number of cells to perform CellPhoneDB analysis. For the IB1 sample[5], the time between baseline and on-treatment sampling is 180 days.

Statistical analysis

Differential Gene Analysis

Within each immune cell type, we first selected genes that are expressed in at least 25% of the cells in either of the two populations under comparison and then applied DESeq2 v1.30.1 to the raw counts in the single-cell data to identify differentially expressed genes between groups of interest. The design matrix only included a factor for the comparison groups (HD, MBL or CLL), without a factor for the individual patents within a group. For the MBL vs. HD comparison, we compared all cells from 4 MBL samples to 2 HD samples; the same design matrix setup was used for CLL vs HD. For CLL vs. MBL, we investigated each patient individually and compared cells from CLL stage to cells from MBL stage. The criteria to define significant differential genes were: 1) the absolute value of average $\log_2$ fold change > 0.6; 2) adjusted p value < 0.05.

To account for patient variance within each comparison group, we performed pseudo-bulk differential gene analysis to confirm the single-cell differential gene analysis results. We first aggregated raw counts for each specific cell type from each single sample, and filtered genes with less than 5 counts. To address the zero-inflation that we observed from our dataset, we applied a zero-inflated negative binomial-based wanted variation extraction method (ZINB-WaVE) to identify and down-weight the excess zeros[6]. Then, we applied the DESeq2 least likelihood test (minmu=1e-6, minRep=Inf) and selected differentially expressed genes with an adjusted p value < 0.05. Again, for the MBL vs. HD comparison, we compared 4 MBL samples to 2 HD samples; the same design matrix setup was used for CLL vs HD. For CLL vs. MBL, we included the factor of patient ID (MBL-CLL1, 2, 3, or 4) along with the comparison condition (MBL or CLL) in the design matrix to account for paired sample comparison.

Cell Type Proportion Analysis

To prevent patient-specific effects, we calculated the weighted average of each cell type number across samples and then calculate the proportion. To evaluate the statistical significance, we performed Welch's t test for each cell type proportion across different groups and defined significant proportion difference with nominal p-value < 0.5.

Interactome Analysis

The cell-cell interaction network was generated using CellPhoneDB v2.1.7 [7] based on the ligand–receptor pairs displaying significant cell-type specificity. For each analysis, we separated the HD cells and patient cells under each cell type and performed CellPhoneDB at the same time to compare the ligand-receptor enrichment under different conditions. We selected the significant differential ligand-receptor pair between HD and patients based on the following criteria: 1) negative $\log_{10}$(p-value) of one group >3 and the other group <1; 2) mean expression of ligand-receptor pair ≥ 2 or < 0.8. Because p-value indicated the enrichment of each ligand-receptor pair, we generated the enrichment heatmap based on the difference in -log10(p-value) from 2 groups to demonstrate whether the interaction is enriched or depleted from one condition to the other. Same analysis was performed for the comparison between individual patient and healthy donors. For the two patients with treatment, we performed the same interactome analysis by comparing the post-ibrutinib sample to the pre-ibrutinib sample.

Data availability

Single cell transcriptome data will be submitted to NCBI's Database of Genotypes and Phenotype (dbGaP; https://www.ncbi.nlm.nih.gov/gap) under study number Phs002705.v1.

SUPPLEMENTARY METHODS REFERENCES

1 Zheng G. X., Terry J.M., Belgrader P., *et al.* Massively parallel digital transcriptional profiling of single cells. *Nat Commun*. 2017; **8:**14049.

2 Massoni-Badosa R. Iacono G., Coutinho C. et al. Sampling time-dependent artifacts in single-cell genomics studies. *Genome Biol*. 2020;21(1):112

3 Hao Y., Hao S., Andersen-Nissen E., *et al*. Integrated analysis of multimodal single-cell data. *Cell*. 2021;184(13):3573-3587.e29.

4 Rendeiro A.F., Krausgruber T., Fortelny N., *et al.* Chromatin mapping and single-cell immune profiling define the temporal dynamics of ibrutinib in CLL. *Nat Commun*. 2020;11(1):577.

5 Gutierrez C., Al'Khafaji A.M., Brenner E., et al. Multifunctional barcoding with ClonMapper enables high-resolution study of clonal dynamics during tumor evolution and treatment. *Nature Cancer*. 2021; **2**:758–772.

6 Van den Berge K., Perraudeau F., Soneson C., et al. Observation weights unlock bulk RNA-seq tools for zero inflation and single-cell applications. *Genome Biol*. 2018;19(1):24.

7 Efremova M., Vento-Tormo M., Teichmann S.A., Vento-Tormo R. CellPhoneDB: inferring cell–cell communication from combined expression of multi-subunit ligand–receptor complexes. *Nat Protoc*. 2020;15(4), 1484-1506.